

Parton Shower Effects on W and Z Production via Vector Boson Fusion at NLO QCD

Franziska Schissler, Dieter Zeppenfeld

*Institute for Theoretical Physics, Karlsruhe Institute of Technology, 76128 Karlsruhe,
Germany*

Abstract

We present the implementation of electroweak Zjj and Wjj production via vector boson fusion with fully leptonic decays at NLO QCD in the POWHEG framework. These processes represent an important background to Higgs searches in vector boson fusion, but they also can be seen as signal processes to study anomalous triple vector boson couplings as well as the impact of a central jet veto. Observables related to the third jet are sensitive to the parton shower which is used, a fact which is demonstrated by a comparison between PYTHIA, the standard angular-ordered HERWIG++ shower and the new p_T -ordered Dipole Shower in HERWIG++.

1 Introduction

With the discovery of a new boson at both ATLAS [1] and CMS [2] we have taken one step closer to the understanding of electroweak symmetry breaking. To achieve this goal, one needs to measure the couplings of this new boson to known Standard Model (SM) particles very precisely. Therefore, both signal and background processes must be understood in detail. In order to give reliable predictions for distributions at hadron colliders, it is mandatory to work at next-to-leading order (NLO) QCD and, if possible, interface this calculation with a parton shower to keep track of additional soft and collinear radiation. Up to now, there exist two prescriptions to match a NLO calculation to parton showers: MC@NLO [3] and POWHEG [4]. We will focus on the latter. The POWHEG method was implemented in a fully flexible program named POWHEG-BOX [5] which equips the users with all subroutines needed to match their fixed-order NLO calculation to a parton shower.

In case of the SM Higgs boson, there already exists such a POWHEG-BOX implementation for gluon fusion in association with zero jets [6], one and two jets [7] and vector boson fusion (VBF) [8]. VBF results in a very specific collider signature with one forward and one backward jet with a large rapidity gap between them which can be used to efficiently suppress background stemming from QCD-induced processes. To study this signature in data, one can look at a W or Z boson produced in VBF [9] and apply for instance central jet veto (CJV) techniques [10] to this kind of processes. Since the cross section is higher for electroweak gauge boson production in VBF than for Higgs production, one can test the theoretical predictions for these processes before going to the real Higgs signal. Therefore, we implemented Wjj and Zjj production in VBF with subsequent leptonic decays in the POWHEG-BOX to give a NLO prediction which can be interfaced with parton showers. The fixed-order α_s corrections to the cross section were already calculated in [11] and we find good agreement with the already existing electroweak Zjj -implementation in the POWHEG-BOX [12]. The QCD induced Zjj production is also part of the POWHEG-BOX [13] and can be used to test the efficiency of VBF cuts for background-suppression.

One goal of this work is to gain experience in interfacing an existing NLO code at fixed order in α_s with the POWHEG-BOX. The processes explained in detail in this publication offer enough complexity to study the compatibility of VBFNLO [14], a fully flexible parton level Monte Carlo program for NLO QCD corrected cross sections and distributions, and the POWHEG-BOX. The future plan is to make more processes implemented in VBFNLO available in the POWHEG-BOX. Additionally, we turn our attention to the influence of the parton shower on the studied processes. To this end, we study the p_T -ordered shower in PYTHIA [15] as well as the vetoed, angular-ordered shower in HERWIG++ [16] and the new p_T -ordered HERWIG++-Dipole Shower [17], in the following just called DS++. From these predictions we can estimate the influence of truncation to an angular ordered shower.

This paper is organized as follows: In Section 2 we review the details of the numerical calculation of all three processes, focusing on the subtleties of the matching between VBFNLO and the POWHEG-BOX. In Section 3 we will give results of our calculation,

showered with PYTHIA, HERWIG++ and DS++. Conclusions are given in Section 4.

2 Details of the Implementation

To interface the parton-level calculation of VBFNLO for Zjj and Wjj production via VBF with shower Monte-Carlo programs we use the publicly available POWHEG-BOX framework [5]. This package equips the user with all needed subroutines to go from a fixed-order NLO calculation in QCD to event files in the LesHouches format [18] which then can be interfaced with a truncated shower. To this end, the POWHEG-BOX asks for the following ingredients:

- The Born squared matrix elements \mathcal{B} for each partonic subprocess. The spin-correlated matrix elements are not needed here since there are no external gluons at tree level.
- The Born color structure in the limit of a large number of colors.
- The phase space for the Born process, see Section 2.2.
- The real emission squared matrix elements.
- The finite part of the interference term between the Born and virtual amplitude.
- The flavor structures of the Born and real emission subprocesses. We used tagging of the different fermion lines as described in [8]. This means that same flavor fermions on the upper and lower quark line internally get a different flavor (tag) to keep them distinct. These tags are only used to assign the possible radiation regions, which are searched for automatically within the POWHEG-BOX.

The details of the implementation of these ingredients will follow below.

The local subtraction terms needed to render the cross section finite are provided by the POWHEG-BOX in the FKS framework [19]. An automated check of all singular regions associated with one specific parton is performed and provides a good check for the flavor structures as well as the ratio between Born and real terms in the infrared (IR) region. Since the POWHEG-BOX offers the possibility to generate fixed leading-order (LO) and NLO distributions with user-defined cuts, a cross check with fixed-order calculations performed with VBFNLO is possible and provides a strong check for the validation of the implementation.

After these checks the POWHEG-BOX generates events in the LesHouches format from the POWHEG-Sudakov factor which can be interfaced with any p_T -ordered shower like PYTHIA and DS++ or to a truncated angular-ordered shower. Since HERWIG++ is an angular-ordered shower, one has to veto radiation harder than the real emission from the matrix element [4]. This option is implemented in HERWIG++. However, one needs a so-called truncated shower to account for additional wide angle, soft radiation. This feature

is not present in the current HERWIG++ release. To estimate the effect of this additional soft radiation, we compare HERWIG++ to the p_T -ordered DS++ in our analysis.

2.1 Matrix elements

The matrix elements were adopted from the VBFNLO implementation explained in detail in [11]. Some sample diagrams for the Born and real emission contributions for Wjj -production are shown in Figures 1 and 2.

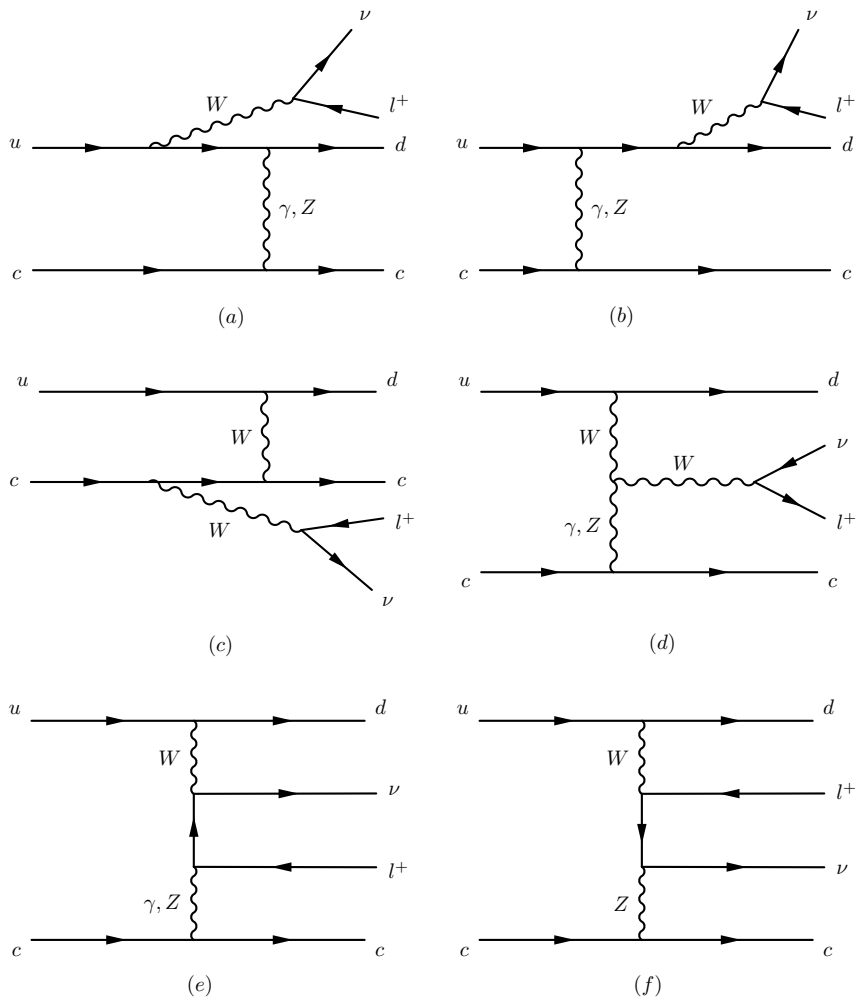


Figure 1: LO diagrams contributing to Wjj production with subsequent leptonic decay. (a)-(d) show resonant graphs, non-resonant graphs like (e) and (f) were also included.

When talking of Vjj -production ($V = W^\pm$ or Z), we mean on the one hand the resonant production of the vector boson with leptonic decay, where off-shell effects are fully taken into account through a modified version of the complex mass scheme [20] with real $\sin^2 \theta_W$ and a Breit-Wigner integration of the propagator over the whole phase space. On the

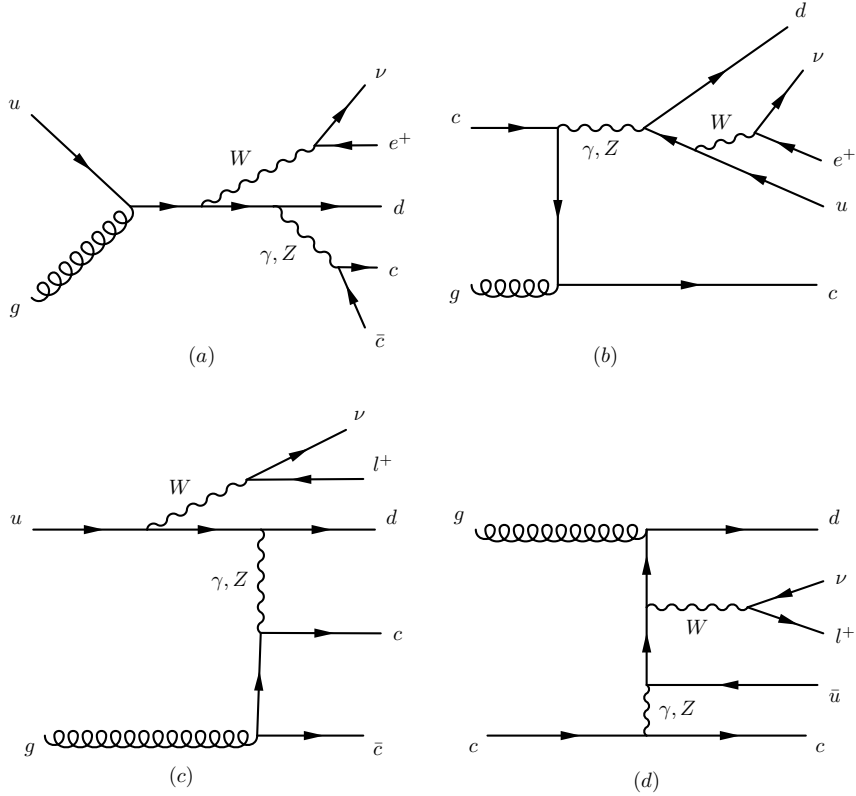


Figure 2: Real emission diagrams for W production via VBF: (a) and (b) are strongly suppressed in the VBF region and can be omitted, (c) and (d) show sample diagrams for gluon-induced amplitudes. Diagrams with final state gluons are obtained by crossing.

other hand, we also take non-resonant production of the leptons into account, see Figure 1 (e), (f). For Zjj -production, we also take a γ^* with subsequent leptonic decay into account. Fermion masses were set to zero throughout and b -quarks in the initial state were neglected. Also, the Cabibbo-Kobayashi-Maskawa matrix was set to the unit matrix. This is no approximation to the calculation as long as the flavor of the jets is not tagged and quark masses are neglected.

In Figure 2 (a) and (b), both (virtual) vector bosons are time-like and contain one vector boson which decays into a quark-anti-quark pair. This is a real emission contribution to WZ production and treated as a separate process. This type of diagrams is therefore not considered here. More details on the used approximations can be found in [11].

One problem in the POWHEG-BOX implementation is the presence of one (Wjj) or even two (Zjj) t -channel photons already at LO. Consequently, the Born cross section is divergent if integrated over the whole phase space, though, of course, it is well defined with normal jet definition cuts. To avoid these singularities, amplitudes which contain a t -channel photon with virtuality $Q^2 < 4 \text{ GeV}^2$ are suppressed with a large damping factor, as already used in [12]. At NLO, the $Q^2 < 4 \text{ GeV}^2$ cut affects the real emission contributions, as long as photon induced processes, which absorb the divergence via the

photon pdf, are not taken into account. In the following the missing $p\gamma \rightarrow VjjX$ piece is considered as a separate electroweak contribution to Vjj production and, since these contributions are quite small when typical VBF cuts are imposed, they were neglected.

2.2 Phase space

In our implementation, there exist three possibilities to evaluate the Born phase-space integral. The standard procedure maps the random numbers given by the integration routines to the physical momenta, adopted from [12]. Since the Born contributions are divergent in certain regions of the phase space, one can impose a cut on the two tagging jets, which can be changed by the user. The invariant dilepton mass for Zjj -production is required to be above 20 GeV by default, thus avoiding the $\gamma^* \rightarrow l^+l^-$ singularity at $Q^2 = 0$ for massless leptons.

As already used in [12] and originally described in [21], there also exists the possibility to use a Born-suppression factor $F(\Phi_n)$ instead of the generation cut on the jets' p_T described above. One possible choice for $F(\Phi_n)$ is

$$F(\Phi_n) = \left(\frac{p_{T,j_1}^2}{p_{T,j_1}^2 + \Lambda_{p_{T_j}}^2} \right)^k \left(\frac{p_{T,j_2}^2}{p_{T,j_2}^2 + \Lambda_{p_{T_j}}^2} \right)^k. \quad (2.1)$$

This factor vanishes whenever a singular region in the Born phase space Φ_n is reached. The underlying Born kinematics are then generated in the POWHEG-BOX according to a modified \bar{B} function,

$$\bar{B}_{\text{supp}} = \bar{B}(\Phi_n)F(\Phi_n). \quad (2.2)$$

The parameters $\Lambda_{p_{T_j}} = 10$ GeV and $k = 2$ can be changed by the user. The resulting events have to be reweighted by a factor $1/F(\Phi_n)$.

To speed up the generation of POWHEG events it is also possible to use unweighted events generated by VBFNLO as phase-space generator¹. The main advantages of this approach is that, first of all, the integration over the Born variables and the optimization of the grid with respect to the underlying Born kinematics can be omitted, since the unweighted events are already flat in the (Born) phase space. These unweighted events can therefore be seen as the perfect LO phase-space generator. Only the integration over the three variables of the real emission has to be handled by the integration routine. To use this option, unweighted events were generated using VBFNLO. Each event i which survived the unweighting procedure was reweighted by the factor

$$J_i = \frac{\sigma_{LO}}{\left(\left| \mathcal{M}_B \left(\Phi_n^{(i)} \right) \right|^2 \text{pdf} \left(\Phi_n^{(i)} \right) \right)},$$

the Born cross section over the respective numerical value of the squared Born matrix element including pdfs. This factor J_i is exactly the Jacobi factor of the Born phase

¹This option can be used by setting the variable `Phasespace` to 2 in the `powheg.input` file.

space. A Monte Carlo integration over N reweighted events then reproduces the Born cross section:

$$\begin{aligned} \frac{1}{N} \sum_{i=1}^N J_i |\mathcal{M}_B(\Phi_n^{(i)})|^2 \text{pdf}(\Phi_n^{(i)}) &= \frac{1}{N} \sum_{i=1}^N \frac{\sigma_{LO}}{|\mathcal{M}_B(\Phi_n^{(i)})|^2 \text{pdf}(\Phi_n^{(i)})} |\mathcal{M}_B(\Phi_n^{(i)})|^2 \text{pdf}(\Phi_n^{(i)}) \\ &= \sigma_{LO}. \end{aligned} \tag{2.3}$$

For the numerical analysis shown in Section 3 we used this third method.

2.3 Checks

To check the implementation, all matrix elements were compared phase-space pointwise with the existing VBFNLO subroutines. With this method, the evaluated couplings and modified routines were validated. Agreement from 11 to 15 digits was found. It was also verified that the subtraction and the real emission terms cancel in the singular limit. Another important check is the agreement of differential fixed-order NLO distributions. All tested distributions agree between the POWHEG-BOX and VBFNLO implementation within statistical errors of at most 1 %. The validation of the use of unweighted events was done by comparing cross sections and distributions at fixed order and after event generation using the three different options to generate the phase space. Good agreement within the statistical errors was found. For Zjj production, we also compared our implementation to [12] using generation cuts in the phase space generator. Matrix elements were compared phase-space pointwise and agreement at the level of 10 relevant digits was found. Cross sections and distributions agree within the statistical uncertainties at NLO and after event generation.

3 Numerical Results

For our numerical analysis for the LHC with center-of-mass energy of 8 TeV we operate with the CT10 pdf set [22] with $\alpha_s(M_Z) = 0.11798$ as implemented in the LHAPDF package [23]. For the calculation of the electroweak couplings we use the input parameters $M_W = 80.398$ GeV, $M_Z = 91.1876$ GeV and the Fermi constant $G_F = 1.16637 \cdot 10^{-5}$ GeV⁻¹. From these parameters the total widths of the electroweak gauge bosons are calculated to be $\Gamma_Z = 2.5084$ GeV and $\Gamma_W = 2.0977$ GeV. The QED fine structure constant is $\alpha_{QED} = 1/132.341$ and the weak mixing angle is $\sin^2 \theta_W = 0.2226$. Partons are recombined into jets according to the anti- k_T algorithm [24] provided by the FASTJET-package [25] with a default distance parameter $R = 0.5$.

For the numerical analysis presented below we use the following inclusive cuts: We require that the two highest p_T jets, called tagging jets, satisfy

$$p_{T,j}^{tag} > 30 \text{ GeV}. \tag{3.1}$$

All observable jets, from the NLO calculation or the Shower, are demanded to have

$$p_{T,j} > 20 \text{ GeV}, \quad (3.2)$$

as well as rapidity

$$|y_j| < 4.5. \quad (3.3)$$

To have well-observable leptons in the central region of the detector, they should obey

$$p_{T,l} > 20 \text{ GeV} \quad \text{and} \quad |y_l| < 2.5. \quad (3.4)$$

Since in Zjj -production, the process $\gamma^*jj \rightarrow l^+l^-jj$ is included as well, one is forced to impose a cut on the invariant mass of the leptons to avoid singularities:

$$m_{ll} > 20 \text{ GeV}. \quad (3.5)$$

All leptons should be well separated from each other and from the jets, assured by

$$\Delta R_{ll} > 0.1 \quad \text{and} \quad \Delta R_{jl} > 0.4, \quad (3.6)$$

where $\Delta R_{ij} = \sqrt{(y_i - y_j)^2 + (\phi_i - \phi_j)^2}$.

Due to the color singlet exchange in the t -channel, the two tagging jets are widely separated in rapidity and usually lie in opposite detector hemispheres. Additionally, the decay products of the weak boson tend to be located in the rapidity gap between the two tagging jets. This special configuration can be used to suppress QCD backgrounds, which have a higher jet activity in the central detector. We therefore demand the typical VBF-cuts

$$m_{jj} > 600 \text{ GeV}, \quad \Delta y_{jj}^{tag} > 4, \quad y_{j1}^{tag} \times y_{j2}^{tag} < 0 \quad \text{and} \quad y_{j,tag}^{min} + 0.2 < y_l < y_{j,tag}^{max} - 0.2. \quad (3.7)$$

The factorization and renormalization scale is set to the produced vector boson's mass $\mu_F = \mu_R = M_V$.

In the following we will discuss W^+jj production with decay into the leptons of the first family. The main findings are the same for W^-jj and Zjj production so only plots for the W^+jj case will be shown. Since we are mostly interested in the effects of the three parton showers, PYTHIA, HERWIG++ and DS++, hadronisation and underlying event simulations were not taken into account. We used PYTHIA-version 6.4.25 with the Perugia 0-tune (Feb 2009) and HERWIG++-version 2.6.1a for the standard shower and for DS++. The cross sections with the VBF-cuts mentioned above are shown in Table 1. Figure 3 shows the invariant mass of the two tagging jets and the transverse momentum of the charged lepton for PYTHIA, HERWIG++ and DS++ in comparison to the fixed order NLO prediction of VBFNLO. As expected, the parton showers have no effect on these observables except for a slight change in the normalization due to the different total cross sections. This change comes from events which pass the cuts in a fixed order calculation but migrate slightly by parton shower effects to phase space regions which are not

	W^+jj	W^-jj	Zjj
NLO	(253.9 ± 0.3) fb	(134.4 ± 0.2) fb	(24.47 ± 0.07) fb
VBFNLO	(254.0 ± 0.1) fb	(134.6 ± 0.1) fb	(24.48 ± 0.02) fb
PYTHIA	(251.0 ± 0.8) fb	(131.7 ± 0.5) fb	(24.48 ± 0.18) fb
HERWIG++	(249.8 ± 0.8) fb	(131.2 ± 0.5) fb	(24.08 ± 0.18) fb
DS++	(245.2 ± 0.8) fb	(128.0 ± 0.5) fb	(23.56 ± 0.18) fb

Table 1: Cross sections for electroweak Vjj production including VBF-cuts (3.1-3.7) with subsequent decay of the vector boson into the first lepton family. The NLO cross section was obtained with the new POWHEG-BOX implementation and matches the VBFNLO prediction. PYTHIA and HERWIG results include parton shower.

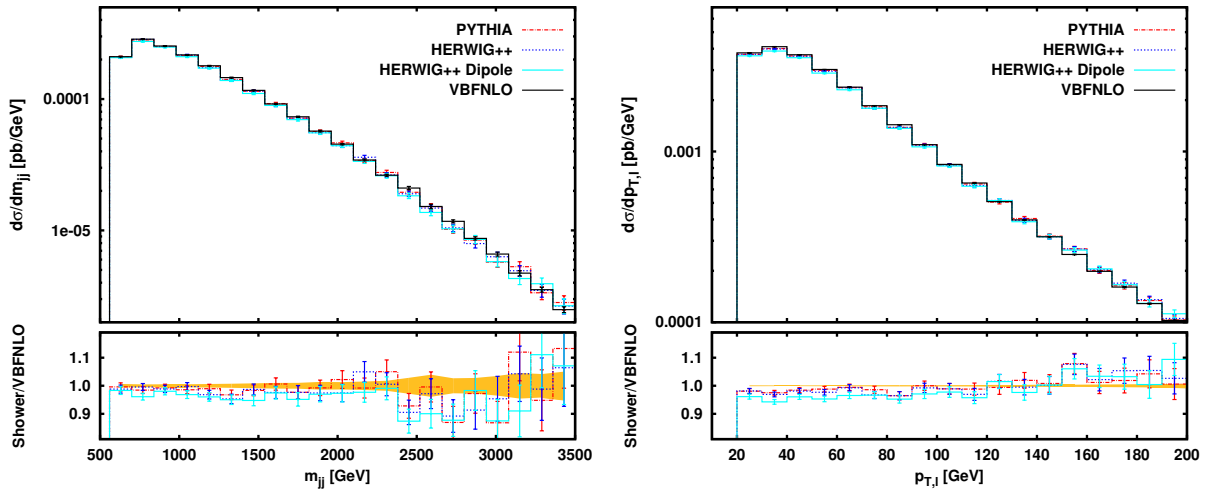


Figure 3: Differential cross-section of the invariant tagging jet mass (left) and the transverse momentum of the charged lepton (right) of the POWHEG-prediction compared to the fixed order curves of VBFNLO (black solid line). The (red) dashed-dotted line shows the prediction of the POWHEG result showered with PYTHIA, the (blue) dotted line corresponds to HERWIG++ and the (turquoise) solid line to DS++. The error bars show the statistical error of the integration, the yellow error band in the ratio plot gives the statistical error on the fixed-order NLO result.

incorporated within the cuts. Also, other observables constructed from the four-momenta of the tagging jets or the leptons are not affected by the parton showers, the VBF signature of the events is therefore preserved.

Differences occur in the differential distributions of the third hardest jet, whose matrix elements are only LO accurate. Figure 4 shows the p_T -spectrum of the third jet and its location relative to the tagging jets,

$$y_3^* = y_{j_3} - (y_{j_1} + y_{j_2})/2. \quad (3.8)$$

For the plot on the left hand side the cut on the transverse momentum of the third jet was lowered to $p_{T,j_3} > 1$ GeV, whereas the right plot contains the usual VBF-cuts (3.1)-(3.7).

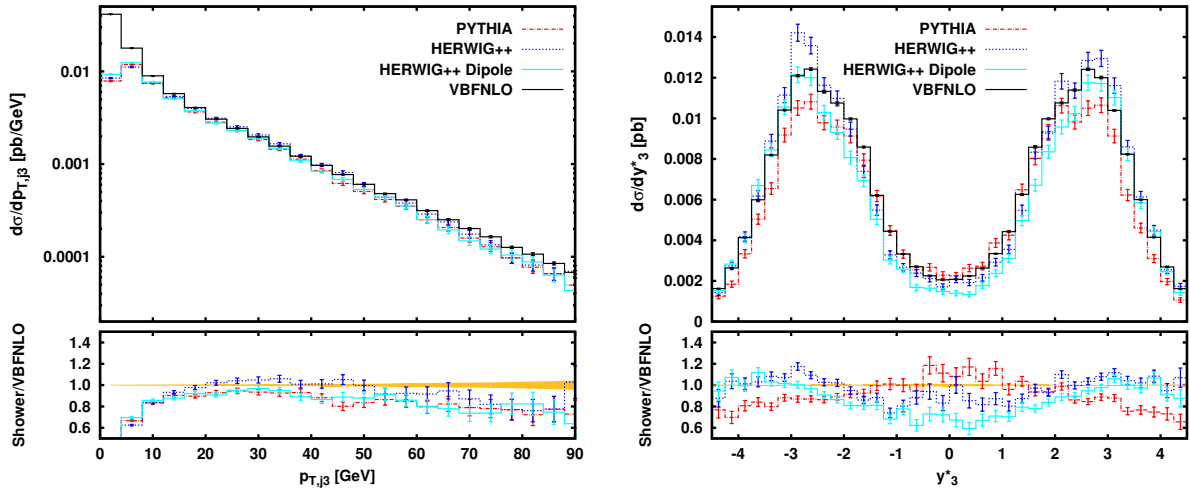


Figure 4: Differential distribution of the transverse momentum of the third jet with $p_{T,j_3} > 1$ GeV (left) and the variable y_3^* (3.8) (right) including all cuts, comparing the predictions of the three parton showers to the fixed order distributions of VBFNLO. The line styles are assigned as in Figure 3.

In the low p_T region, the damping of the soft divergence due to the Sudakov factor can be observed for all three parton showers. Between 20 and 50 GeV, HERWIG++ predicts more jets than PYTHIA, but matches the NLO prediction, whereas PYTHIA and DS++ are in good agreement. In the tail of the distributions for hard jets with $p_T \gtrsim 75$ GeV, all three parton showers have lower rates than the NLO distribution. This comes from additional hard and/or wide angle radiation which can lead to additional jets which are not re-clustered in the direction of the parent parton.

Even bigger differences occur for the differential distribution of the variable y_3^* (3.8), see the right plot of Figure 4. With the $\Delta y_{jj}^{\text{tag}} > 4$ cut, the two tagging jets peak at $|y_j^{\text{tag}}| \approx 2.7$, so $|y_3^*| \lesssim 2.7$ typically corresponds to the rapidity gap between the tagging jets and $|y_3^*| \gtrsim 2.7$ to the third jet being positioned between the tagging jets and the beam axis. PYTHIA tends to radiate more into the rapidity gap and additionally underestimates the region between the tagging jets and the beam axis, whereas HERWIG++ and DS++ behave the opposite way.

This effect gets even more pronounced if one varies the distance parameter R of the anti- k_T algorithm or lowers the p_T -cut on the third jet, see Figure 5. The differences of the showers are due to the fact that PYTHIA tends to emit more soft partons, whereas HERWIG++ and DS++ preferentially emit partons in the collinear region between the tagging jets and the beam axis and therefore pull the third jet in that direction. If one lowers the p_{T,j_3} -cut, Figure 5 left, PYTHIA fills the region between the tagging jets with soft partons. These can recombine into the third-hardest jet which then ends up in the rapidity gap. However, the y_3^* distribution for HERWIG++ and DS++ is fairly unaffected by the lower p_{T,j_3} -cut. The shape of the curves stay the same compared to the NLO prediction. The collinear region is well described by the two showers, whereas the

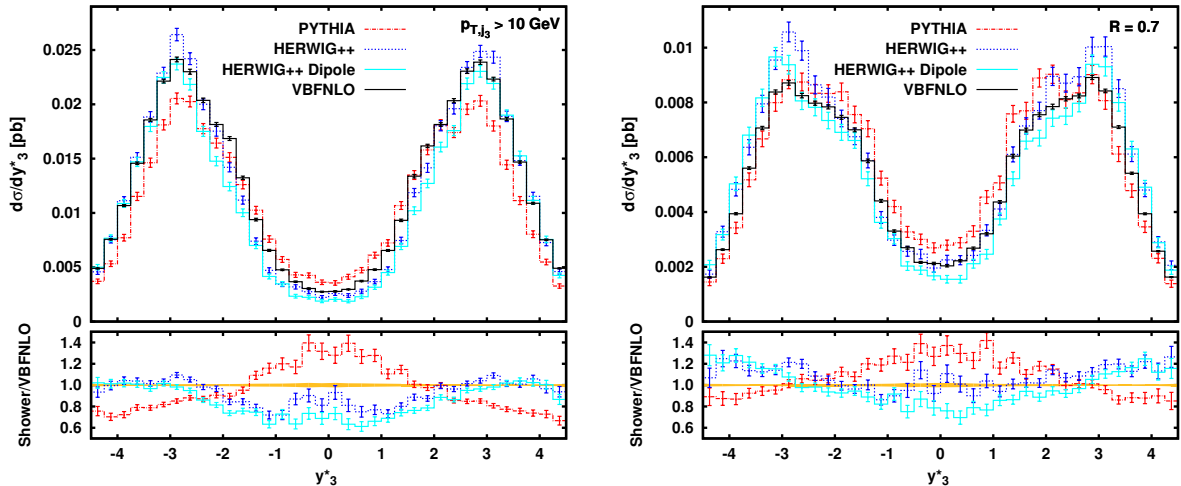


Figure 5: Left: Differential y_3^* -distribution (3.8) for $p_{T,j_3} > 10$ GeV. Right: Differential y_3^* -distribution for $R = 0.7$. The line styles are assigned as in Figure 3.

rate in the central region is too low.

A similar effect can be seen when the distance parameter R of the anti- k_T algorithm is increased. As an example the right hand side of Figure 5 shows the y_3^* distribution for $R = 0.7$ instead of the default $R = 0.5$. In PYTHIA, the jet activity in the rapidity gap rises compared to the fixed-order NLO prediction since more soft and/or collinear partons are clustered in the third jet. This increases the possibility of the third jet to be detected. In contrast, HERWIG++ and DS++ tend to radiate collinearly between the tagging jets and the beam remnant which leads to jets with high $|y_3^*|$. This collinear radiation does not affect the shape of y_3^* when lowering the p_{T,j_3} -cut, it does however change by increasing R (Figure 5, right). For $R = 0.7$, the two HERWIG++ showers produce more jets in the collinear region than VBFNLO. Since HERWIG++ and DS++ predict the same behavior for the y_3^* -variable, one can conclude that the difference between HERWIG++ and PYTHIA is not caused by wide-angle, soft radiation which is included in DS++. Therefore, truncated shower effects play a minor role. The difference between the two HERWIG++-showers and PYTHIA rather seems to depend on how the available phase space is filled with soft and collinear radiation.

Additionally, the jets obtained with PYTHIA are broader than the HERWIG++ and DS++ ones, which is also responsible for the different behavior of the three showers in the rapidity gap. This can be seen from the differential jet shape [26] $\rho(r)$ of the third jet, which is a measure for the jet energy flow. Following Reference [27] we define the differential jet shape as

$$\rho(r) = \frac{1}{\Delta r} \sum_{parton \in j_3} \frac{p_{T,parton}(r - \Delta r/2, r + \Delta r/2)}{p_{T,j_3}} \quad (3.9)$$

with r ranging between $\frac{\Delta r}{2}$ and $R - \frac{\Delta r}{2}$. $p_{T,parton}(r_1, r_2)$ denotes the p_T of partons in an

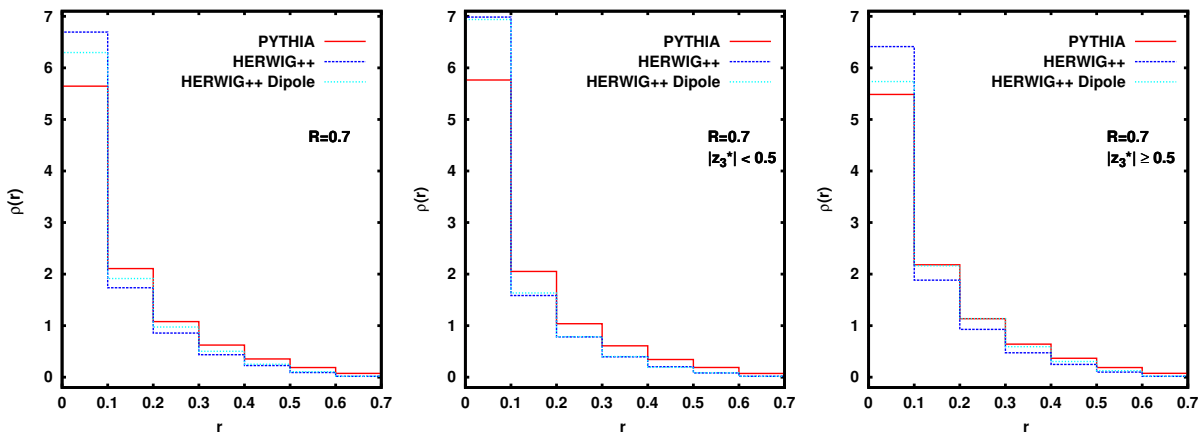


Figure 6: $\rho(r)$ distribution for $R = 0.7$ for different regions of the third jet. The line styles are assigned as in Figure 3.

annulus between radii r_1 and r_2 , i.e. $r_1 \leq r = \sqrt{(\phi_{j_3} - \phi_{parton})^2 + (y_{j_3} - y_{parton})^2} < r_2$. The sum runs over all partons which are recombined into the third jet. We use $\Delta r = 0.1$ here and the normalization assures that $\int_0^R \rho(r) dr = 1$. In Figure 6, the averaged $\rho(r)$ is plotted for the third jet with distance parameter $R = 0.7$ for different areas of the phase space. To distinguish the position of the third jet, we use the variable

$$z_3^* = \frac{y_3^*}{|y_{j_1} - y_{j_2}|}. \quad (3.10)$$

The tagging jets are localized at $|z_3^*| = 0.5$, $|z_3^*| < 0.5$ corresponds to the rapidity gap and $|z_3^*| > 0.5$ to the region between the tagging jets and the beam axis.

On the left hand side of Figure 6, the differential jet shape $\rho(r)$ is plotted in the whole allowed phase space. Clearly, PYTHIA produces broader jets than HERWIG++ and DS++. The probability to find partons with $r > 0.1$ which are clustered into the third jet are considerably higher than for the other two parton showers. The middle plot shows $\rho(r)$ for a third jet falling in the rapidity gap between the two tagging jets, in the right plot the jet falls into the collinear region between the tagging jets and the beam axis. It is noticeable that much of the difference between HERWIG++ and PYTHIA stems from jets in the central region. This matches the observations made before and is also correlated on how the available phase space for additional radiation is filled: collinear radiation leads to narrow jets, whereas soft, wide-angle radiation is rather uncorrelated to the parton where it is radiated off and can therefore broaden the jet. For PYTHIA, this effect is large for jets in the central region (Figure 6, middle), whereas the differential jet shape for jets between the tagging jets and the beam axis is almost the same for PYTHIA and DS++. In this region, the jet behaves almost like in an inclusive jet sample, which is reasonably well described by all three showers [27]. Compared to HERWIG++, DS++ predicts slightly broader jets. This can be explained by additional soft radiation due to a low IR cut-off on the Sudakov factor in DS++. By increasing this cut-off, agreement in the differential jet shape and the rate of third jet can be obtained.

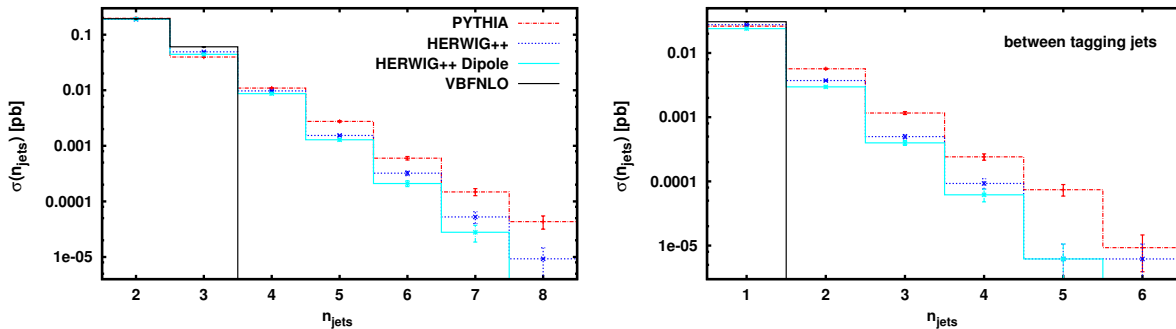


Figure 7: Jet multiplicity with the standard cuts (3.1)-(3.7) for jets in the whole allowed phase space (left) and in the rapidity gap between the tagging jets (right). The line styles are assigned as in Figure 3.

The broadening of the third jet in the central region is also the reason why, over a large range of p_T , the p_{T,j_3} -curve of PYTHIA lies below the HERWIG++ prediction (see Figure 4, left). PYTHIA radiates wide-angle partons which are not clustered into the jet and therefore take away part of the original p_T from the parent parton. In HERWIG++ many radiated partons get clustered along the axis of the parent parton to the third jet as well as additional radiation from the two tagging jets. This can be seen in the p_{T,j_3} -distribution for large distance parameters $R \geq 0.5$, where it exceeds even the NLO prediction. To see the effect of radiation coming from the tagging jets also in PYTHIA, the distance parameters R has to be increased even more. The difference between HERWIG++ and DS++ comes from the different normalization of the two curves. As mentioned before, DS++ is known to radiate more soft partons which can lead to a lower rate of the third jet once a minimum p_T and a maximum rapidity threshold on the tagging jets is set.

All this has consequences for CJV techniques, since the multiplicity of jets between the tagging jets is quite different for PYTHIA, HERWIG++ and DS++, as shown in Figure 7. The first three jets, which come from the hard matrix elements, are reasonably well described by all three showers, whereas additional jets, which solely come from the showers, show big differences. PYTHIA radiates off more partons which survive the jet criteria (3.2, 3.3, 3.6), both in the whole allowed phase space and in the rapidity gap between the two tagging jets. One other important conclusion of this work is that HERWIG++, as a vetoed angular-ordered shower shows the same behavior as its p_T -ordered sibling DS++. Therefore, at least for the processes studied here, the effect of truncation can be neglected.

4 Conclusions

We implemented Wjj and Zjj production via VBF in the POWHEG-BOX. The POWHEG framework allows to interface an NLO calculation with parton showers. One basic finding is that, as expected, the shape of the distributions of the two tagging jets and the leptons are mostly independent of parton shower effects. Small changes appear in the overall cross

sections which arise from migration of some events to phase space regions which are not incorporated within the cuts. In contrast, the distribution of the third jet, which is only LO accurate, is sensitive to the details of the parton shower in use. Dependent on the cuts used, the effect on third jet distributions can easily be of the order of 30 – 40%. Since the standard angular-ordered HERWIG++ shower and the new p_T -ordered HERWIG++-Dipole Shower are in good agreement, we expect the effects of additional wide-angle soft radiation, which is missing in the vetoed angular-ordered shower, to be small. However, there exist sizable differences between PYTHIA and HERWIG++. This is due to the fact that PYTHIA predicts broader (third) jets than HERWIG++, especially in the central region of the detector. These stem from soft, wide-angle radiation. In HERWIG++, the third jet tends to be located in the region outside the rapidity gap due to additional small-angle radiation. The difference between the two HERWIG++-showers and PYTHIA seems to be caused by the filling of the available phase space for additional radiation by the respective shower: PYTHIA tends to fill the rapidity gap between the two tagging jets with rather soft partons, while HERWIG++ leaves the rapidity gap essentially unaltered and radiates additional partons preferentially in the collinear region between the tagging jets and the beam axis.

These differences between the three shower predictions reflect remaining uncertainties of available NLO predictions. They are mostly present in the distributions of the third jet, since it is only LO accurate, and have to be taken into account when comparing the predictions to data.

Acknowledgments

We thank Stefan Gieseke for many useful discussions concerning the differences between HERWIG++ and PYTHIA and for carefully reading the manuscript. F.S. was supported by the "Graduiertenkolleg 1694, Elementarteilchenphysik bei höchster Energie und höchster Präzision". The Feynman diagrams have been drawn using the package FEYNMF [28].

References

- [1] G. Aad *et al.* [ATLAS Collaboration], Phys. Lett. B **716**, 1 (2012) [arXiv:1207.7214 [hep-ex]].
- [2] S. Chatrchyan *et al.* [CMS Collaboration], Phys. Lett. B **716**, 30 (2012) [arXiv:1207.7235 [hep-ex]].
- [3] S. Frixione and B. R. Webber, JHEP **0206**, 029 (2002) [hep-ph/0204244].
- [4] P. Nason, JHEP **0411**, 040 (2004) [hep-ph/0409146];
S. Frixione, P. Nason and C. Oleari, JHEP **0711**, 070 (2007) [arXiv:0709.2092 [hep-ph]].

- [5] S. Alioli, P. Nason, C. Oleari and E. Re, JHEP **1006**, 043 (2010) [arXiv:1002.2581 [hep-ph]].
- [6] S. Alioli, P. Nason, C. Oleari and E. Re, JHEP **0904**, 002 (2009) [arXiv:0812.0578 [hep-ph]].
- [7] J. M. Campbell, R. K. Ellis, R. Frederix, P. Nason, C. Oleari and C. Williams, JHEP **1207**, 092 (2012) [arXiv:1202.5475 [hep-ph]].
- [8] P. Nason and C. Oleari, JHEP **1002**, 037 (2010) [arXiv:0911.5299 [hep-ph]].
- [9] The CMS Collaboration, CMS-PAS-FSQ-12-019;
- [10] Y. L. Dokshitzer, V. A. Khoze and S. I. Troian, in Proceedings of the 6th International Conference on Physics in Collisions, (1986) ed. M. Derrick (World Scientific, 1987) p. 365;
 J. D. Bjorken, Phys. Rev. D **47**, 101 (1993);
 V. D. Barger, R. J. N. Phillips and D. Zeppenfeld, Phys. Lett. B **346**, 106 (1995) [hep-ph/9412276];
 D. L. Rainwater, R. Szalapski and D. Zeppenfeld, Phys. Rev. D **54** (1996) 6680 [hep-ph/9605444];
 V. Khoze, M. Ryskin, W. Stirling *et al.*, Eur.Phys.J. C26 (2003) 429440, [hep-ph/0207365].
- [11] C. Oleari and D. Zeppenfeld, Phys. Rev. D **69**, 093004 (2004) [hep-ph/0310156].
- [12] B. Jäger, S. Schneider, G. Zanderighi, S. Schneider and G. Zanderighi, JHEP **1209**, 083 (2012) [arXiv:1207.2626 [hep-ph]].
- [13] E. Re, JHEP **1210**, 031 (2012) [arXiv:1204.5433 [hep-ph]].
- [14] K. Arnold, M. Bähr, G. Bozzi, F. Campanario, C. Englert, T. Figy, N. Greiner and C. Hackstein *et al.*, Comput. Phys. Commun. **180**, 1661 (2009) [arXiv:0811.4559 [hep-ph]];
 K. Arnold, J. Bellm, G. Bozzi, F. Campanario, C. Englert, B. Feigl, J. Frank and T. Figy *et al.*, [arXiv:1207.4975 [hep-ph]];
 K. Arnold, J. Bellm, G. Bozzi, M. Brieg, F. Campanario, C. Englert, B. Feigl and J. Frank *et al.*, [arXiv:1107.4038 [hep-ph]].
- [15] T. Sjöstrand, S. Mrenna and P. Z. Skands, JHEP **0605**, 026 (2006) [hep-ph/0603175].
- [16] M. Bähr, S. Gieseke, M. A. Gigg, D. Grellscheid, K. Hamilton, O. Latunde-Dada, S. Plätzer and P. Richardson *et al.*, Eur. Phys. J. C **58**, 639 (2008) [arXiv:0803.0883 [hep-ph]];
 K. Arnold, L. d’Errico, S. Gieseke, D. Grellscheid, K. Hamilton, A. Papaefstathiou, S. Plätzer and P. Richardson *et al.*, [arXiv:1205.4902 [hep-ph]].

- [17] S. Plätzer and S. Gieseke, JHEP **1101**, 024 (2011) [arXiv:0909.5593 [hep-ph]];
S. Plätzer and S. Gieseke, Eur. Phys. J. C **72**, 2187 (2012) [arXiv:1109.6256 [hep-ph]].
- [18] E. Boos, M. Dobbs, W. Giele, I. Hinchliffe, J. Huston, V. Ilyin, J. Kanzaki and K. Kato *et al.*, [hep-ph/0109068].
- [19] S. Frixione, Z. Kunszt and A. Signer, Nucl. Phys. B **467**, 399 (1996) [hep-ph/9512328];
S. Frixione, Nucl. Phys. B **507**, 295 (1997) [hep-ph/9706545].
- [20] A. Denner, S. Dittmaier, M. Roth and D. Wackerath, Nucl. Phys. B **560**, 33 (1999) [hep-ph/9904472].
- [21] S. Alioli, P. Nason, C. Oleari and E. Re, JHEP **1101**, 095 (2011) [arXiv:1009.5594 [hep-ph]].
- [22] H. -L. Lai, M. Guzzi, J. Huston, Z. Li, P. M. Nadolsky, J. Pumplin and C. -P. Yuan, Phys. Rev. D **82**, 074024 (2010) [arXiv:1007.2241 [hep-ph]].
- [23] M. R. Whalley, D. Bourilkov and R. C. Group, [hep-ph/0508110], see also <http://hepforge.cedar.ac.uk/lhapdf/> .
- [24] M. Cacciari, G. P. Salam and G. Soyez, JHEP **0804**, 063 (2008) [arXiv:0802.1189 [hep-ph]].
- [25] M. Cacciari and G. P. Salam, Phys. Lett. B **641**, 57 (2006) [hep-ph/0512210];
M. Cacciari, G. P. Salam and G. Soyez, Eur. Phys. J. C **72**, 1896 (2012) [arXiv:1111.6097 [hep-ph]].
- [26] S. D. Ellis, Z. Kunszt and D. E. Soper, Phys. Rev. Lett **69** 3615 (1992).
- [27] G. Aad *et al.* [Atlas Collaboration], Phys. Rev. D **83**, 052003 (2011) [arXiv:1101.0070 [hep-ex]].
- [28] T. Ohl, Comput. Phys. Commun. **90**, 340 (1995) [hep-ph/9505351].